Valproic Acid Prolongs Survival Time of Severe Combined Immunodeficient Mice Bearing Intracerebellar Orthotopic Medulloblastoma Xenografts

Qin Shu,[1] Barbara Antalffy,[2] Jack Meng Feng Su,[3] Adekunle Adesina,[2] Ching-Nan Ou,[2] Torsten Pietsch,[4] Susan M. Blaney,[3] Ching C. Lau,[3] and Xiao-Nan Li[1]

Abstract

Purpose: To develop novel orthotopic xenograft models of medulloblastoma in severe combined immunodeficient mice and to evaluate the *in vivo* antitumor efficacy of valproic acid.

Experimental Design: Orthotopic xenografts were developed by injecting 10^3 to 10^5 tumor cells from four medulloblastoma cell lines (D283-MED, DAOY, MHH-MED-1, and MEB-MED-8A) into the right cerebellum of severe combined immunodeficient mice. Animals were then examined for reproducibility of tumorigenicity, cell number-survival time relationship, and histopathologic features. Tumor growth was monitored *in vivo* by serially sectioning the xenograft brains at 2, 4, 6, and 8 weeks postinjection. Valproic acid treatment, administered at 600 μg/h for 2 weeks via s.c. osmotic minipumps, was initiated 2 weeks after injection of 10^5 medulloblastoma cells, and treated and untreated animals were monitored for differences in survival. Changes in histone acetylation, proliferation, apoptosis, differentiation, and angiogenesis in xenografts were also evaluated.

Results: Tumorigenicity was maintained at 100% in D283-MED, DAOY, and MHH-MED-1 cell lines. These cerebellar xenografts displayed histologic features and immunohistochemical profiles (microtubule-associated protein 2, glial fibrillary acidic protein, and vimentin) similar to human medulloblastomas. Animal survival time was inversely correlated with injected tumor cell number. Treatment with valproic acid prolonged survival time in two (D283-MED and MHH-MED-1) of the three models and was associated with induction of histone hyperacetylation, inhibition of proliferation and angiogenesis, and enhancement of apoptosis and differentiation.

Conclusion: We have developed intracerebellar orthotopic models that closely recapitulated the biological features of human medulloblastomas and characterized their *in vivo* growth characteristics. Valproic acid treatment of these xenografts showed potent *in vivo* anti-medulloblastoma activity. These xenograft models should facilitate the understanding of medulloblastoma pathogenesis and future preclinical evaluation of new therapies against medulloblastoma.

Medulloblastoma, the most common malignant brain tumor of childhood, is still associated with significant morbidity and mortality, particularly in infants and young children (1, 2). The development of clinically relevant preclinical models of medulloblastoma is essential not only for enhancing our understanding of their biology but also for evaluating the therapeutic potential of novel treatment approaches.

Standard models for assessing efficacy of anticancer drugs, such as *in vitro* human cancer cell lines and s.c. xenograft tumor models (3, 4), do not accurately replicate the cellular complexity, microenvironment, and extracellular compartment of the corresponding tumors, particularly tumors of the central nervous system. Moreover, preclinical results obtained from such s.c xenograft models may overpredict the efficacy of candidate drugs for tumors of the central nervous system because intratumoral drug exposure in patients may be much lower as a result of restricted drug delivery by the blood-brain barrier. Thus, there is growing skepticism about the value of traditional preclinical models for *in vivo* preclinical drug testing (5) and increasing efforts are devoted to developing animal models that will faithfully simulate the biology and genetic alterations in human cancers.

In addition to genetically engineered animal models that hold the promise of recapitulating important features of human oncogenesis (3, 6–14), substantial progress has been achieved in establishing orthotopic xenografts of multiple

Authors' Affiliations: [1]Laboratory of Molecular Neuro-Oncology, [2]Department of Pathology, and [3]Texas Children's Cancer Center, Texas Children's Hospital, Baylor College of Medicine, Houston, Texas and [4]Department of Neuropathology, University of Bonn Medical Center, Bonn, Germany

Received 12/30/05; revised 5/3/06; accepted 5/11/06.

Grant support: Childhood Brain Tumor Foundation and National Brain Tumor Foundation (X.N. Li), John S. Dunn Research Foundation, Robert J. Kleberg, Jr., and Helen C. Kleberg Foundation, Gillson Longenbaugh Foundation and Cancer Fighters of Houston, Inc. (C.C. Lau).

The costs of publication of this article were defrayed in part by the payment of page charges. This article must therefore be hereby marked *advertisement* in accordance with 18 U.S.C. Section 1734 solely to indicate this fact.

Requests for reprints: Xiao-Nan Li, Laboratory of Molecular Neuro-Oncology, Texas Children's Cancer Center, Texas Children's Hospital, 6621 Fannin Street, MC 3-3320, Houston, TX 77030. Phone: 832-824-4580; Fax: 832-825-4038; E-mail: Xiaonan@bcm.tmc.edu.

doi:10.1158/1078-0432.CCR-05-2849

human cancers (15–23), including glioma (24–27). Orthotopic xenograft models reproduce the microenvironment and biological phenotype of the originating tumor more faithfully than s.c. xenografts and more accurately predict the clinical activity of novel drugs (3, 4, 15).

For human medulloblastomas, previous orthotopic xenograft models were established by transplanting human medulloblastoma cells into mouse cerebrum, and these intracerebral xenograft models have been used to evaluate the antitumor activity of therapeutic agents (28–31), investigate the growth suppressive effects of basic fibroblastic growth factor (32), and optimize magnetic resonance imaging (33). Injection of a medulloblastoma cell line (MHH-MED-1) into the cistern magna of nude rats has also been reported (34). Because human medulloblastomas normally occur in cerebellum, some researchers have started to inject medulloblastoma cells into mouse cerebellum. In a recent study, DAOY cells were inoculated into mouse cerebellum to establish cerebellar tumors that were subsequently treated with reovirus (35). However, systematic development and comprehensive characterization of multiple intracerebellar orthotopic medulloblastoma xenograft models simulating different histologic subtypes of human medulloblastomas have not previously been reported.

In the current study, we describe the establishment of intracerebellar medulloblastoma xenograft models in severe combined immunodeficient (SCID) mice from four medulloblastoma cell lines and the utilization of these models in the preclinical evaluation of anti-medulloblastoma activities of valproic acid, an established anticonvulsant drug that has recently been identified as a histone deacetylase inhibitor (36). Our previous studies *in vitro* and in s.c. medulloblastoma xenografts showed that valproic acid possesses potent antitumor activities by inhibiting cell proliferation, promoting apoptosis, and inducing cellular senescence and differentiation (37). Because valproic acid can cross the blood-brain barrier and is orally bioavailable with a long half-life in children (9-18 hours), a rigorous preclinical assessment of its antitumor efficacy in mice bearing intracerebellar xenograft tumors would provide valuable information for future clinical application of valproic acid in children with medulloblastomas.

Materials and Methods

Cell lines. D283-MED and DAOY cell lines were obtained from the American Type Culture Collection (Manassas, VA; refs. 28–30); MHH-MED-1 and MEB-MED-8A cell lines were originally developed by Pietsch et al. (38, 39). These medulloblastoma cell lines were maintained in DMEM supplemented with 10% fetal bovine serum (Mediatech, Herndon, VA).

Heterotransplantion into right cerebellum of SCID mice. All animal experiments were conducted according to an Institutional Animal Care and Use Committee–approved protocol. Rag2 SCID mice were bred and maintained in a specific pathogen–free animal facility in Texas Children's Hospital. Food and water were provided *ad libitum*. To establish intracerebellar xenograft models, 6- to 10-week-old mice were anesthesized with sodium pentobarbital (50 mg/kg); after which, a small skin incision (1 mm) was made and a burr hole (0.7 mm in diameter) created with microsurgical drill (Fine Science Tools, Foster City, CA). Tumor cells (10^3-10^5) were suspended in 2 μL of culture medium and injected slowly through the burr hole into the right cerebellar hemisphere (1 mm to the right of the midline, 1 mm posterior to the coronal suture, and 3 mm deep) using a 10-μL, 26-gauge Hamilton Gastight 1701 syringe needle that was inserted perpendicular to the cranial surface. The animals were monitored daily until signs of neurologic deficit developed, at which time they were euthanized and their brains removed for histopathologic analysis. Tumor size was estimated by quantifying the maximum cross-sectional area from digitized images captured from H&E-stained sections using ImageJ.[5] Mean ± SE values were calculated from three consecutive images per mouse (n = 5 mice per group). Animals that died or developed neurologic deficit(s) within 24 hours of tumor cell injection were included in the calculation of surgical death rate.

In vivo *treatment of xenografts with valproic acid.* Valproic acid (2-propyl-pentanoic acid) was purchased from Sigma (St. Louis, MO) and dissolved in 0.9% sodium chloride solution to a final concentration of 600 mg/mL. Valproic acid (600 mg/mL) was administered via a s.c. implanted ALZET model 2001 osmotic pump (Durect Corporation, Cupertino, CA) that continuously released valproic acid at a constant rate of 1 μL/h. S.c. pumps were implanted in animals anesthesized as described above. After shaving the skin over the implantation site, a 0.8-cm midscapular incision was made on the back of the animal. A hemostat was inserted into the incision to spread the s.c. tissue to create a pocket for a pump. A filled pump was inserted into the pocket and the incision was closed with wound clips or sutures. The animals were treated with valproic acid for a total of 14 days by replacing the first pump with a second filled pump 7 days after initial implantation. Animal body weights were monitored weekly. Plasma concentrations of total valproic acid were analyzed with the Abbott AxSYM valproic acid assay reagent system (Abbott Laboratories, Abbott Park, IL) using anti–coagulated blood (50-75 μL) collected from clipped mouse tails. Plasma valproic acid concentrations were monitored throughout the 14 days of treatment and maintained in the range of 70 ± 15 μg/mL.

Measurement of histone hyperacetylation, proliferation, differentiation, and angiogenesis. Immunohistochemistry was done on 5-μm paraffin sections using a Vectastain Elite kit (Vector Laboratories, Burlingame, CA) per instructions of the manufacturer. The antibodies used in this study included monoclonal antibodies against hyperacetylated histone H3 (1:300) and H4 (1:500; Upstate Labs, Charlottesville, VA), Ki-67 (Abcam, Inc., Cambridge, CA; 1:20), microtubule-associated protein 2 (MAP-2; 1:200; Abcam, Inc.), synaptophysin (1:200) and glial fibrillary acidic protein (GFAP; 1:200; Dako, Carpinteria, CA), and polyclonal antibodies against von Willebrand factor (Chemicon International, Inc., Temecula, CA) and vascular endothelial cell growth factor (VEGF; 1:200; Santa Cruz Biotechnology, Santa Cruz, CA). After slides were incubated with primary antibodies for 90 minutes at room temperature, the appropriate biotinylated secondary antibodies (1:200) were applied and incubated for 30 minutes. The signal was developed using the 3,3′-diaminobenzidine substrate kit for peroxidase. The intensity of immunohistochemical staining was assessed using a numerical scale (0, no expression; +, low expression; ++, moderate expression; and +++, strong expression). Ki-67- and VEGF-positive cells were counted under 10 high-power fields and expressed as percent of total cells counted. Microvessel density was determined by calculating the average number of vessels smaller than 8 RBC, as identified by von Willebrand factor staining, which were present in >10 high power fields randomly selected in four consecutive sections (numbered 1-4), two of which (nos. 2 and 4) were counterstained with hematoxylin to facilitate tumor identification.

Apoptosis assay. Apoptosis was assessed by the terminal deoxynucleotidyl transferase–mediated dUTP nick end labeling method using the In Situ Cell Death Detection Kit, AP (Boehringer Mannheim GmbH, Boehringer, Germany) as previously described (40). Following deparaffinization and rehydration, slides were incubated with 50 μL of the

[5] http://rsb.info.nih.gov/ij.

reaction mixture for 90 minutes. Cell nuclei were counterstained with 4′,6-diamidino-2-phenylindole. A minimum of 10 images (10 × 20) were captured from three sections under fluorescence microscopy and the number of positive cells was counted.

Statistical analysis. Animal survival times were analyzed with SigmaStat using log-rank survival analysis and graphed with SigmaPlot. Differences in tumor size, cell proliferation (Ki-67 positivity), apoptosis, and VEGF expression between the valproic acid–treated and control groups were analyzed using the *t* test.

Results

Tumorigenicity of medulloblastoma cell lines. MEB-MED-8A was the only cell line that failed to generate intracerebellar tumors in SCID mice. Injection of as few as 10^3 D283-MED, DAOY, or MHH-MED-1 cells resulted in 100% formation of intracerebellar (ICb) tumors. These tumor xenografts were subsequently referred to as ICb-D283, ICb-DAOY, and ICb-MED-1, respectively. Only 9 of the 254 (3.7%) mice died from possible surgical injuries.

In vivo *growth of intracerebellar orthotopic xenograft models.* To monitor the *in vivo* growth patterns of medulloblastoma xenografts, five mice from each of the three models were euthanized every 2 weeks postinjection until they developed neurologic deficit (~8 weeks). Progressive enlargement of the cerebella was visible by gross examination starting from the 4th week, and expanding tumors breaking through the cerebellar surface were apparent by the 6th week. By the time an animal became moribund or paralyzed, a huge intracerebellar tumor could easily be seen, and there was frequently none or only a thin layer of normal cerebellar tissue remaining (data not shown).

Microscopic examination showed that, at 2 weeks postinjection, the tumors were ~1 mm in size, all located deep within the central region of the right cerebellum (Fig. 1A, *a*). These tumors then expanded and invaded surrounding cerebellar tissues, leading to destruction of the normal cerebellar architecture and eventual replacement of the cerebellum by tumor (Fig. 1A, *a-d*). In all three models, there was no capsule or membrane surrounding the intracerebellar tumors. No tumor formation in the injection track was observed.

Histopathologic features of the orthotopic xenograft tumors. Tumor histology was reviewed by our institutional pediatric neuropathologist (A.A.). At 2 weeks postinjection, ICb-D283 tumor cells were composed of a monomorphic population of small blue cells, with a few cells showing prominent nucleoli and open chromatin and occasional "cell wrapping" and mitoses. After 4 weeks, a more extensive subpopulation of large cells with increasingly open chromatin and large nucleoli became more prominent. These cells often formed distinct clusters and showed early signs of invading adjacent cerebellar neuropil. After >8 weeks of growth, the cerebellum was nearly replaced by tumor cells; "cell wrapping," an aggressive histologic feature, became more frequent; multinucleated cells were occasionally seen; and large areas of necrosis and leptomeningeal spread were easily observed. Overall, ICb-D283 most closely resembled the large-cell variant of human medulloblastomas (Fig. 1B, *e-g*).

The ICb-DAOY xenografts resembled anaplastic human medulloblastoma (Fig. 1B, *h-j*). These cells also had open chromatin and prominent nucleoli but showed extensive pleomorphism and frequent mitosis. After 8 weeks of *in vivo* growth, the severity and extent of anaplasia and nuclear molding became more readily appreciable.

The ICb-MED-1 tumors displayed histologic features resembling classic human medulloblastoma (Fig. 1B, *k-m*). These primitive-appearing and monomorphic cells had small nucleoli (micronucleoli), scant cytoplasm, and little evidence of differentiation. After prolonged *in vivo* growth, the tumor cell uniform morphology and neuropil-type stroma remain unchanged.

Correlation of number of injected tumor cells and mouse survival time. To examine the effect of the number of injected cells on mouse survival time, three groups of mice ($n = 5$ per group) were injected with 10^3, 10^4, and 10^5 cells. As shown in Fig. 2A, animal survival time inversely correlated with the number of injected cells. Mice receiving 10^3 cells survived significantly longer than those injected with 10^4 or 10^5 cells, regardless of cell type ($P < 0.05$). Differences in median survival time between mice injected with 10^4 cells and those injected with 10^5 cells were also significant in ICb-DAOY and ICb-MED-1 animals ($P < 0.05$), but not in ICb-D283 animals ($P > 0.05$).

In all three models, reducing the number of injected tumor cells by 10- or 100-fold only moderately lengthened survival time, as these increments ranged from 13% in ICb-DAOY ($10^5/10^4$) to 2.8-fold in ICb-MED-1 ($10^5/10^3$) mice. These observations suggest that biological factors other than the starting number of tumor cells also contributed to the determination of survival time. Mice injected with identical number of cells all died within a narrow period of time (Fig. 2A). The ratios of SD of survival/mean survival time were <20% in ICb-D283 and <10% in ICb-DAOY and ICb-MED-1 animals. The tight clustering of animal survival times suggests that these tumors maintained similar *in vivo* growth characteristics in SCID mice.

Valproic acid prolongs survival time of SCID mice bearing orthotopic medulloblastoma xenografts. Injected tumor cells were permitted to grow for 2 weeks before start of valproic acid treatment. Differences in animal survival time were used to assess treatment effects. Compared with the control group, mice treated with valproic acid survived significantly longer in two of the three models. The mean survival time was extended from 56 ± 1.63 to 62.9 ± 1.2 days (12.6% increase) in mice bearing ICb-D283 xenografts, and from 74.2 ± 20.5 to 133.8 ± 63.9 days (80% increase) in ICb-MED-1 mice ($P < 0.05$ for both observations). In animals bearing ICb-DAOY xenografts, only a minor increase of survival time was observed in the valproic acid–treated group relative to controls ($P > 0.05$; Fig. 2B).

Valproic acid inhibits proliferation and induces apoptosis in orthotopic medulloblastoma xenografts. To evaluate the effects of valproic acid treatment on tumor growth, tumor sizes at the end of valproic acid treatment (4 weeks post tumor cell injection) were estimated by measuring the maximum cross-sectional areas on three consecutive digitalized sections of cerebellum/tumor. Compared with the control group, tumors in mice treated with valproic acid were significantly smaller in all three models ($P < 0.05$; Fig. 3A). In those mice that were monitored for survival and euthanized when they became moribund (>8 weeks post injection), we did not observe

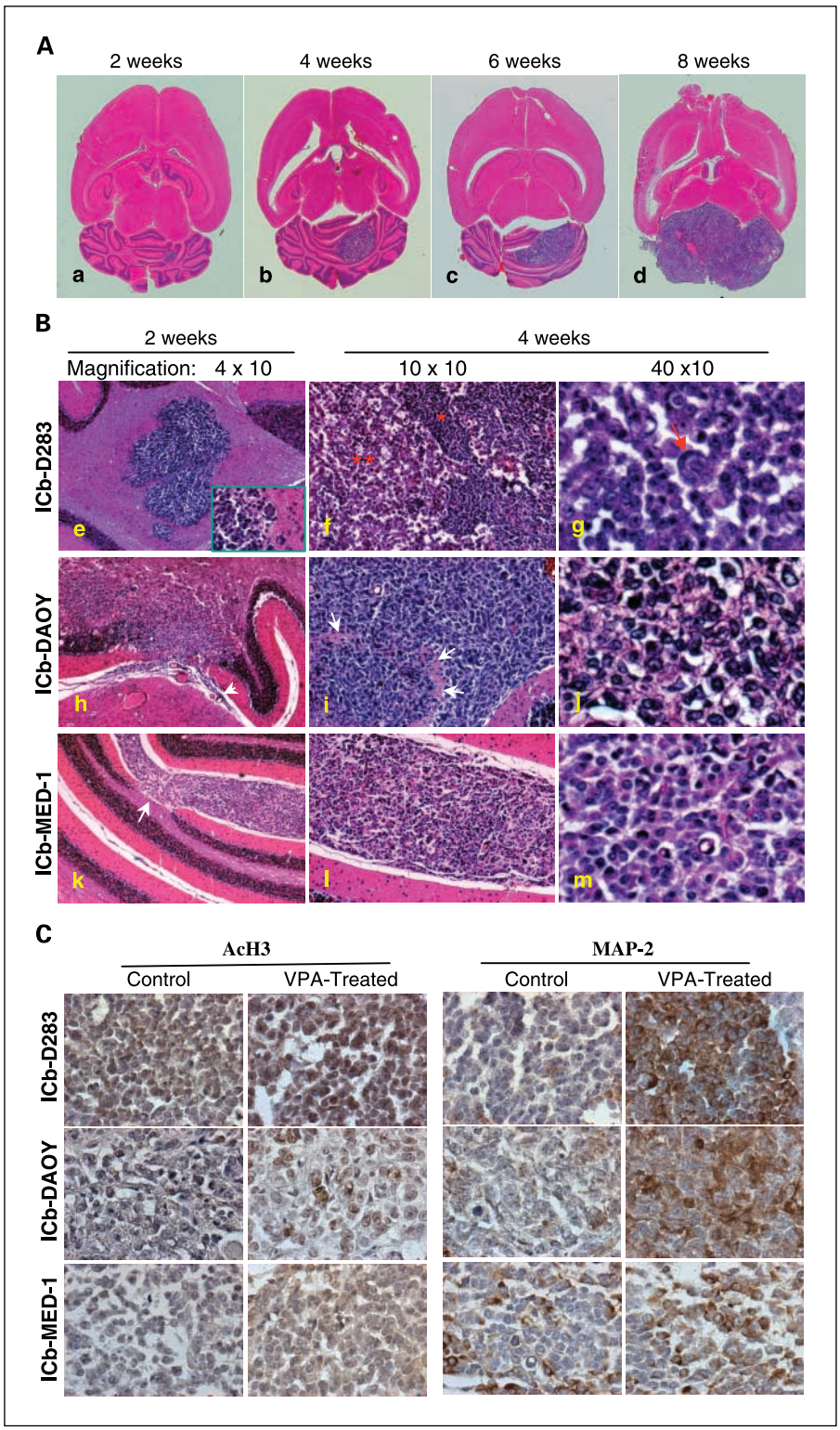

Fig. 1. *In vivo* growth, histologic, and immunohistochemical characteristics of orthotopic medulloblastoma xenograft models in SCID mice. *A*, representative images showing the time course of *in vivo* growth of ICb-D283 xenografts. Mice injected with 10^5 tumor cells in the right cerebellar were euthanized (five mice each) at 2, 4, and 6 weeks postinjection and at the end of experiment when they developed neurologic deficits. The mouse brains were then paraffin embedded, serially sectioned, and stained with H&E (*a-d*). *B*, histologic features of intracerebellar xenografts at 2 and 4 weeks postinjection. For ICb-D283 tumors, early invasion (*e, inset*), the small round blue cells (*), larger, more aggressive-appearing cells (**; *f*), and cell wrapping (*arrow*; *g*) were shown. For ICb-DAOY tumors, early subarachnoidal spread (*arrow head*; *h*), subsequent deep invasion into the surrounding normal folium (*white arrows*; *i*), and striking cellular polymorphism were presented. For ICb-MED-1, early invasion into normal tissues (*k*) and more uniform morphology (*l* and *m*) could be seen. Magnification, 4 × 10 (*e, h*, and *k*), 10 × 10 (*f, l*, and *l*), and 10 × 40 (*g, j*, and *m*). *C*, immunohistochemical analysis of AcH3 and neuronal marker MAP-2 expression induced by valproic acid. Five mice from each model were euthanized at the end of valproic acid treatment (4 weeks post tumor injection; *VPA-Treated*) and compared with the untreated mice (*Control*). Magnification, 10 × 40.

significant differences in tumor sizes. All the animals had extensive tumors that almost completely replaced the normal cerebella.

Changes in tumor cell proliferation were assessed by Ki-67 immunohistochemical staining. As shown in Fig. 3B and D, proliferation rates in untreated xenografts varied substantially, with ICb-MED-1 showing the lowest number of Ki-67-positive cells. Valproic acid treatment resulted in a 73.6% reduction of Ki-67-positive cells in ICb-MED-1 tumors, a 29.4% reduction in ICb-D283 tumors, and a 35.6% reduction in ICb-DAOY tumors (Fig. 3B and D; $P < 0.01$). Increases in apoptosis, as evidenced by increments in terminal deoxynuleotidyl transferase–mediated dUTP nick end labeling–positive cells, were also observed in all three models, and ICb-MED-1 tumors

exhibited the highest level increase of apoptotic cells (Fig. 3C and E; $P < 0.05$).

Valproic acid induces histone (H3 and H4) hyperacetylation in orthotopic medulloblastoma xenografts. We have previously shown histone (H3 and H4) hyperacetylation in both cultured medulloblastoma cells and s.c. xenografts after valproic acid treatment and a correlation between the degree of histone hyperacetylation and drug responsiveness (37). To examine the effect of valproic acid on histone acetylation in orthotopic xenografts, mice treated with or without valproic acid were euthanized at the completion of 2 weeks of valproic acid treatment (4 weeks posttransplantation). Because of the relatively small (<5 mm) tumors following valproic acid treatment, it was technically difficult to dissect an adequate number of pure tumor cells for Western hybridization. Histone hyperacetylation was therefore assessed by immunohistochemical examination using antibodies against hyperacetylated H3 (AcH3) and H4 (AcH4). In ICb-D283 xenografts, prominent increases of both AcH3 and AcH4 were observed, whereas in ICb-MED-1 xenografts, the induction of AcH3 was more pronounced. In ICb-DAOY xenografts, only an intermediate increase in AcH3 was noted (Table 1; Fig. 1C).

Valproic acid induces neuronal differentiation of orthotopic medulloblastoma xenografts. Changes in expressions of markers associated with neuronal or glial differentiation and the intermediate filament vimentin were examined by immunohistochemistry on xenograft tumors at the end of valproic acid treatment. Compared with synaptophysin of which the expression remained low and barely changed, expression of MAP-2 was readily induced by valproic acid in all three models (Table 1). In ICb-D283 and ICb-DAOY xenografts that expressed low levels of MAP-2 proteins before treatment, both the staining intensity and the number of positive cells increased after treatment. In ICb-MED-1 tumors, which were originally with strong (+++) MAP-2 expression, valproic acid treatment increased the positive cells from 50% pretreatment to 75% after treatment (Fig. 1C).

Although induction of glial marker GFAP expression was previously observed in our *in vitro* studies (37, 40), only a few GFAP-expressing cells were seen in the orthotopic xenografts before or after treatment. These GFAP-positive cells, mostly spindle or stellate in shape and located in the peripheral zones between tumor cells and normal mouse brain tissues, are interpreted as reactive astrocytes. Strong (+++) expression of vimentin was readily detected in all untreated tumors and treatment with valproic acid resulted in minimal changes (Table 1).

Valproic acid inhibits angiogenesis in orthotopic medulloblastoma xenografts. To assess the effect of valproic acid on tumor angiogenesis, microvessel density was examined by immunohistochemical staining of the endothelial marker von Willebrand factor. Compared with untreated xenografts in which multiple microvessel could be easily observed, treated xenografts displayed remarkable reduction in microvessel density, particularly in ICb-D283 and ICb-MED-1 xenografts (Fig. 3F and H). Reductions of microvessel density in DAOY xenografts, although statistically significant ($P < 0.05$), were <50%.

To explain the differential angiogenic responses, changes in angiogenic factor VEGF were examined by immunohistochemistry in the same set of xenograft tumors. In ICb-D283 tumors, VEGF-positive cells decreased from 45% to <10% after valproic acid treatment ($P < 0.01$). In untreated ICb-MED-1 tumors, ~10% of the tumor cells were VEGF positive, and treatment with valproic acid caused an insignificant decrease of VEGF expression ($P > 0.05$). Although <20% of tumor cells in ICb-DAOY xenografts expressed VEGF, these cells, however, were almost 10 times larger than those in the ICb-D283 and ICb-MED-1 tumors (Fig. 3G). In contrast to ICb-D283 tumors, treatment with valproic acid failed to significantly reduce the percentage or size of VEGF-expressing cells in ICb-DAOY tumors ($P > 0.05$). These results suggest that the antiangiogenic activity of valproic acid is correlated with the regulation of VEGF expression.

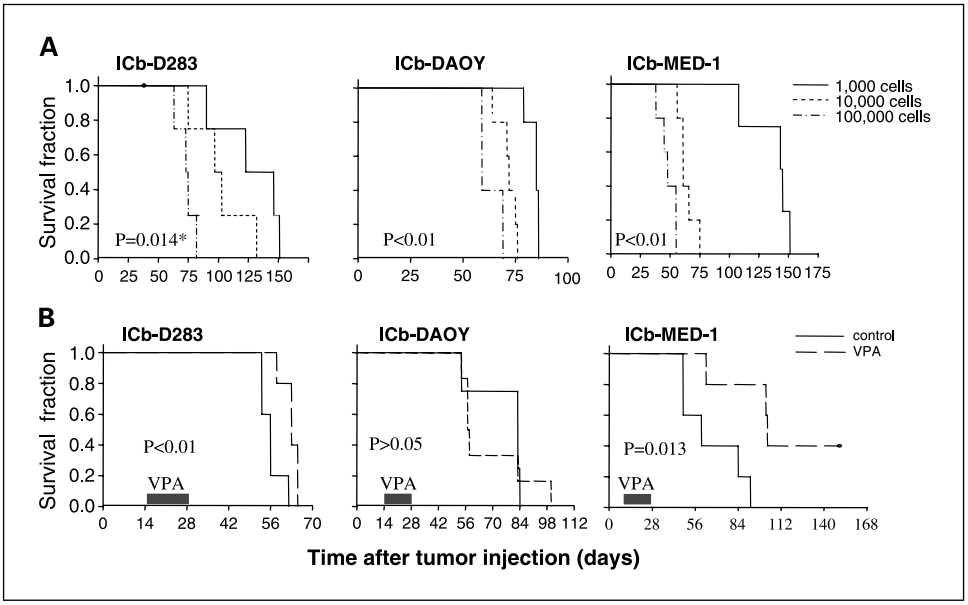

Fig. 2. Log-rank survival analysis of mice bearing intracerebellar medulloblastoma xenografts from D283, DAOY, and MED-1 cell lines. *A*, effect of cell number on animal survival times. For each cell line, three different numbers of tumor cells (10^3, 10^4, and 10^5) were suspended in 2 μL of growth medium and injected into the right cerebellum of five Rag2 SCID mice, respectively. $P < 0.05$, for all group comparisons ($10^3/10^4$, $10^4/10^5$, $10^3/10^5$) except for comparison between mice injected with 10^4 and 10^5 of D283 cells. *B*, effect of valproic acid treatment on animal survival times. Each mouse received injection of 10^5 tumor cells in the right cerebellum. Two weeks later, when solid tumors are formed, systemic treatment with valproic acid was started for a duration of 14 days (*blue bar*) using two s.c. osmotic minipumps that release valproic acid (600 mg/mL) at a constant rate of 1 μL/h (600 μg/h). The control group received no treatment.

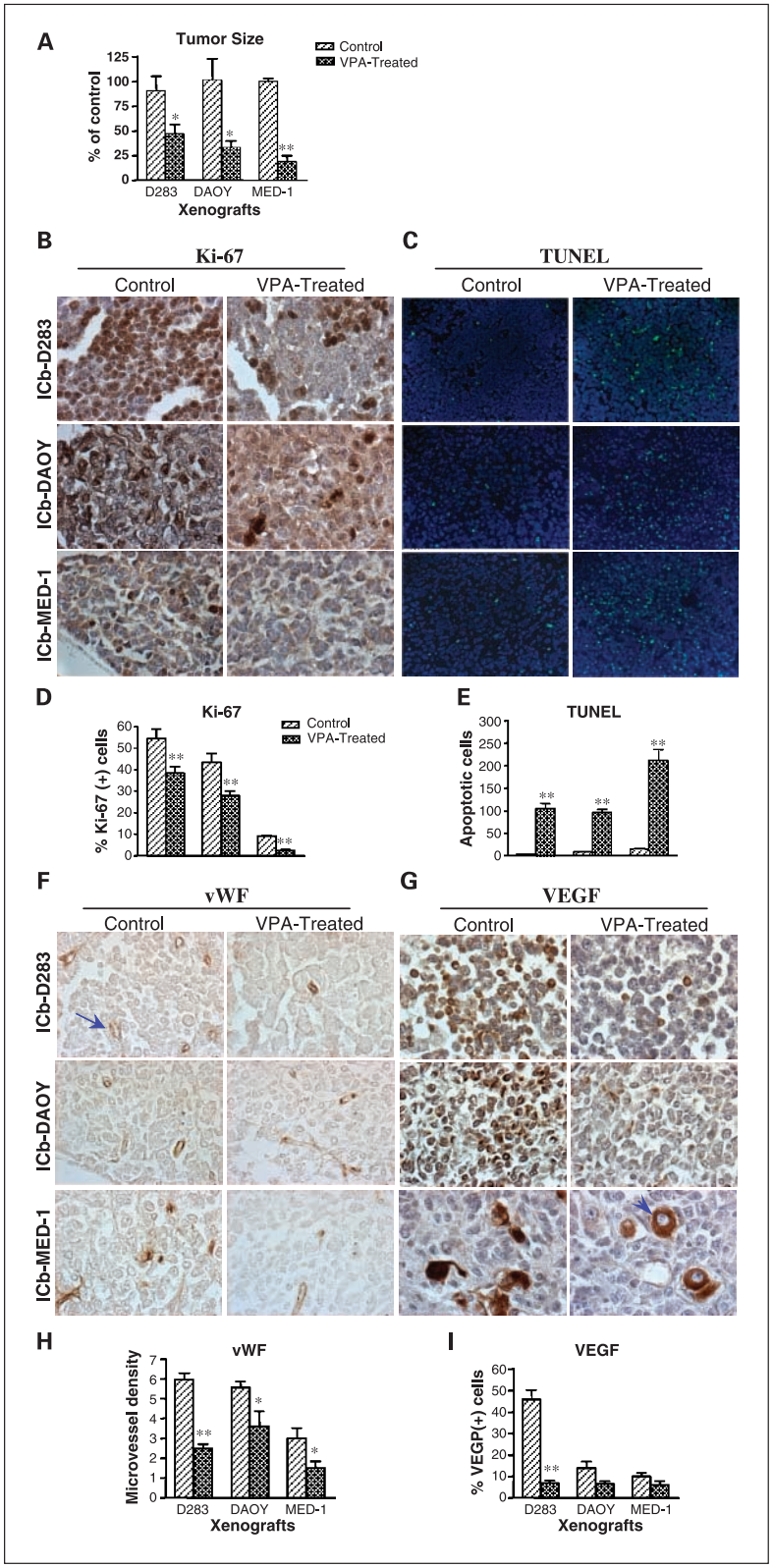

Fig. 3. *In vivo* antitumor activities of valproic acid. Mice bearing intracerebellar xenografts were sacrificed at the end of valproic acid treatment (4 weeks post tumor injection) and compared with the untreated group. *A*, suppression of tumor growth. Tumor size was determined by measuring the maximum cross-sectional areas in at least three consecutive sections for each of the tumors ($n = 5$ per group). Tumor sizes in the treated groups were normalized with the corresponding control groups. *B* and *D*, inhibition of cell proliferation. The proliferative cells identified by immunohistochemical staining with Ki-67 (*B*) were counted in digitally captured images under high-power (10×40) magnification and graphed as the percentage of total cells (*D*). *C* and *E*, induction of apoptosis. Apoptotic cells were detected with terminal deoxynuleotidyl transferase – mediated dUTP nick end labeling assay and counted in digitally captured images under high-power (10×20) magnifications. *F* to *I*, inhibition of angiogenesis. Microvessel density was determined by counting blood vessels (*arrow*) identified by immunostaining with von Willebrand factor (*vWF*; *F*) in digitally captured images under high power (10×40) magnifications (*F* and *H*). Changes of VEGF expression were evaluated by counting the immunopositive cells (*G* and *I*). The VEGF-positive cells in ICb-DAOY (*arrowhead*) were much larger than those in ICb-D283 and ICb-MED-1 tumors. Columns, mean; bars, SE. *, $P < 0.05$; **, $P < 0.01$.

Discussion

In this study, we successfully established three intracerebellar medulloblastoma xenograft models in SCID mice, which, to our knowledge, represent the first set of well-characterized orthotopic medulloblastoma xenograft models. These models displayed reproducible growth rate and animal survival time and exhibited many histopathologic, immunohistochemical,

Table 1. Summary of immunohistochemical examination of histone acetylation (AcH3 and AcH4), markers associated with neuronal (MAP-2 and synaptophysin) and glial (GFAP) differentiation, and intermediate filaments (VMT) in xenografts treated with or without valproic acid

Markers	ICb-D283		ICb-DAOY		ICb-MED-1	
	Untreated	Treated	Untreated	Treated	Untreated	Treated
AcH3	+/−, 30%	+, 90%	+/−, 10%	+, 50%	+, 15%	+, 70%
AcH4	+, 25%	+, 80%	(−)	+, 5%	+, 20%	+, 85%
MAP-2	++, 5%	+++, 30%	+, 20%	++, 70%	+++, 50%	+++, 75%
Synaptophysin	++, 50%	++, 60%	+, 5%	+, 5%	+, 10%	+, 10%
GFAP	(−)	(−)	(−)	(−)	(−)	(−)
VMT	+++, 85%	+++, 80%	+++, 100%	+++, 100%	+++, 90%	+++, 70%

and phenotypic features similar to human medulloblastomas (41, 42). Using these orthotopic models, we showed that treatment with histone deacetylase inhibitor valproic acid significantly prolonged survival time in two of the three xenograft models and resulted in induction of histone hyperacetylation, growth suppression, apoptosis, differentiation, and antiangiogenesis within the xenografts.

One of the advantages of xenograft models is that the kinetics of tumor growth can be predicted (43). Therefore, injections of identical numbers of tumor cells into the same location in the cerebellum would theoretically produce xenografts with comparable growth rates. In the current study, we have shown that all three intracerebellar xenograft models displayed reproducible survival times, and by varying the number of cells injected, we can customize the models to mimic various clinical settings, such as minimal residual disease versus bulky tumors.

The responses of xenografts toward chemotherapy, as measured by changes in animal survival time, are often used to predict clinical efficacy. However, solely using the magnitude of increased survival time may inaccurately predict clinical efficacy of new treatments. For example, reducing the injected tumor cells from 10^5 to 10^3 increased the mean survival by >100 days in ICb-MED-1 mice, whereas a similar reduction in tumor cell number in ICb-DAOY mice only prolonged survival by 20 days (Fig. 2B). Such drastic variabilities in extending survival after similar reductions in tumor burden reflected inherent differences in biological behaviors and *in vivo* growth properties dictated by the underlying genetic background of the three cell lines. Therefore, our established and reproducible cell number-survival time relationship may serve as an objective biological ruler that will not only aid in accurately measuring the antitumor efficacies of future therapeutic strategies but will also help to cross-evaluate the antitumor activities in different models.

In agreement with our previous findings with valproic acid and other histone deacetylase inhibitors *in vitro* and in s.c. xenograft animal models (37, 40), our current study showed that the anti-medulloblastoma activities of valproic acid correlated with increased histone acetylation, suppression of proliferation, induction of apoptosis and differentiation, and inhibition of angiogenesis. The responses of the three orthotopic xenograft models toward valproic acid treatment, however, were variable. In ICb-D283 xenografts, increased apoptosis, induced expression of MAP-2 protein, and inhibited angiogenesis seemed to play major roles, whereas in ICb-MED-1 tumors, suppressed growth index, induced apoptosis, and expression of MAP-2 seemed to be the main mechanisms. In ICb-DAOY xenograft, the initial suppression of cell proliferation and induction of apoptosis did not translate into significant extension of animal survival time, implying that the ICb-DAOY tumor cells regained their proliferation potential after cessation of valproic acid treatment. This result is in agreement with our previous findings in cultured medulloblastoma cells (37) and suggests that long-term treatment may be required to sustain therapeutic efficacy. In addition to the anaplastic histology and the presumed more malignant nature of ICb-DAOY xenografts, many other factors, including the intrinsic genetic differences among the three cell lines (e.g., *p53* mutation and deletion of $p14^{ARF}$, $p15^{INK4B}$, and $p16^{INK4a}$ genes in DAOY cells; refs. 44, 45) and differences in proliferation rate, metastatic potential, and tumor-host interaction (46), might explain the differential responses of these models to valproic acid treatment.

It should be noted that the half-life of valproic acid in mice (0.8 hour) is much shorter than that in humans (9-18 hours). Despite extensive research efforts since 1980s, it remains difficult to maintain clinically achievable plasma valproic acid concentration (100-150 μg/mL) in mice. We attempted different routes of drug delivery, including i.p. injection (up to twice a day), several models of osmotic minipumps with varying release rates (0.25 and 1 μL/h), and different valproic acid concentrations (up to 900 mg/mL; data not shown). The maximum valproic acid levels we were able to maintain were 70 ± 15 μg/mL using osmotic minipumps that released valproic acid (600 mg/mL) at 1 μL/h for 7 days. Despite the possibly subtherapeutic levels of plasma valproic acid, we still observed significant antitumor effects in two of three orthotopic models, and a significant improvement in animal survival time may have been achieved with higher plasma concentrations.

The major limitation of our models is that all of them originated from established cell lines. Although cultured cells provide a stable source of tumor cell supply and ease of manipulation, their inherent disadvantages include the lack of heterogeneity of cell population, uniform growth rate, and possible hyperresponsiveness toward treatment (3–5). One possible solution is to establish orthotopic xenograft models from primary human medulloblastomas by directly injecting freshly resected tumor fragments into mouse cerebella.

Orthotopic models established with histologically intact tumor tissues have been reported to be better in preserving the invasive properties in several human cancers, including gliomas (47–49). Another issue that should also be addressed in future medulloblastoma animal models is the age of animals. The mice in this study were mostly young adults (6-10 weeks old), and the microenvironment of adult cerebella might be biologically different from the developing brains in younger mice, of which the developmental stages may more accurately mirror the pediatric cerebella in which medulloblastomas normally arise (3, 5).

In summary, we have established and characterized three orthotopic xenograft medulloblastoma models in SCID mice and examined the antitumor efficacy of the recently identified histone deacetylase inhibitor valproic acid. Our results provided a strong rationale for future application of these models in the preclinical evaluation of new therapies for medulloblastoma.

References

1. Packer RJ, Rood BR, MacDonald TJ. Medulloblastoma: present concepts of stratification into risk groups. Pediatr Neurosurg 2003;39:60–7.
2. Rood BR, MacDonald TJ, Packer RJ. Current treatment of medulloblastoma: recent advances and future challenges. Semin Oncol 2004;31:666–75.
3. Dyer MA. Mouse models of childhood cancer of the nervous system. J Clin Pathol 2004;57:561–76.
4. Kamb A. What's wrong with our cancer models? Nat Rev Drug Discov 2005;4:161–5.
5. Kerbel RS. Human tumor xenografts as predictive preclinical models for anticancer drug activity in humans: better than commonly perceived-but they can be improved. Cancer Biol Ther 2003;2:S134–9.
6. Holland EC. Mouse models of human cancer as tools in drug development. Cancer Cell 2004;6:197–8.
7. Raffel C. Medulloblastoma: molecular genetics and animal models. Neoplasia 2004;6:310–22.
8. Green JE, Hudson T. The promise of genetically engineered mice for cancer prevention studies. Nat Rev Cancer 2005;5:184–98.
9. Goodrich LV, Milenkovic L, Higgins KM, Scott MP. Altered neural cell fates and medulloblastoma in mouse patched mutants. Science 1997;277:1109–13.
10. Johnson RL, Rothman AL, Xie J, et al. Human homolog of patched, a candidate gene for the basal cell nevus syndrome. Science 1996;272:1668–71.
11. Zurawel RH, Allen C, Wechsler-Reya R, Scott MP, Raffel C. Evidence that haploinsufficiency of Ptch leads to medulloblastoma in mice. Genes Chromosomes Cancer 2000;28:77–81.
12. Wetmore C, Eberhart DE, Curran T. Loss of p53 but not ARF accelerates medulloblastoma in mice heterozygous for patched. Cancer Res 2001;61:513–6.
13. Hallahan AR, Pritchard JI, Hansen S, et al. The SmoA1 mouse model reveals that notch signaling is critical for the growth and survival of sonic hedgehog-induced medulloblastomas. Cancer Res 2004;64:7794–800.
14. Lee Y, McKinnon PJ. DNA Ligase IV suppresses medulloblastoma formation. Cancer Res 2002;62:6395–9.
15. Hoffman RM. Orthotopic metastatic mouse models for anticancer drug discovery and evaluation: a bridge to the clinic. Invest New Drugs 1999;17:343–59.
16. Lang JY, Chen H, Zhou J, et al. Antimetastatic effect of salvicine on human breast cancer MDA-MB-435 orthotopic xenograft is closely related to Rho-dependent pathway. Clin Cancer Res 2005;11:3455–64.
17. Kim S, Park YW, Schiff BA, et al. An orthotopic model of anaplastic thyroid carcinoma in athymic nude mice. Clin Cancer Res 2005;11:1713–21.
18. Zhang X, Galardi E, Duquette M, Delic M, Lawler J, Parangi S. Antiangiogenic treatment with the three thrombospondin-1 type 1 repeats recombinant protein in an orthotopic human pancreatic cancer model. Clin Cancer Res 2005;11:2337–44.
19. Capella G, Farre L, Villanueva A, et al. Orthotopic models of human pancreatic cancer. Ann N Y Acad Sci 1999;880:103–9.
20. Yokoi K, Thaker PH, Yazici S, et al. Dual inhibition of epidermal growth factor receptor and vascular endothelial growth factor receptor phosphorylation by AEE788 reduces growth and metastasis of human colon carcinoma in an orthotopic nude mouse model. Cancer Res 2005;65:3716–25.
21. Hoffman RM. Orthotopic transplant mouse models with green fluorescent protein-expressing cancer cells to visualize metastasis and angiogenesis. Cancer Metastasis Rev 1998;17:271–7.
22. Horiuchi H, Kawamata H, Fujimori T, Kuroda Y. A MEK inhibitor (U0126) prolongs survival in nude mice bearing human gallbladder cancer cells with K-ras mutation: analysis in a novel orthotopic inoculation model. Int J Oncol 2003;23:957–63.
23. Kim SJ, Johnson M, Koterba K, Herynk MH, Uehara H, Gallick GE. Reduced c-Met expression by an adenovirus expressing a c-Met ribozyme inhibits tumorigenic growth and lymph node metastases of PC3-4 prostate tumor cells in an orthotopic nude mouse model. Clin Cancer Res 2003;9:5161–70.
24. Lefranc F, James S, Camby I, et al. Combined cimetidine and temozolomide, compared with temozolomide alone: significant increases in survival in nude mice bearing U373 human glioblastoma multiforme orthotopic xenografts. J Neurosurg 2005;102:706–14.
25. Giannini C, Sarkaria JN, Saito A, et al. Patient tumor EGFR and PDGFRA gene amplifications retained in an invasive intracranial xenograft model of glioblastoma multiforme. Neuro-oncol 2005;7:164–76.
26. Eyupoglu IY, Hahnen E, Buslei R, et al. Suberoylanilide hydroxamic acid (SAHA) has potent anti-glioma properties *in vitro, ex vivo* and *in vivo*. J Neurochem 2005;93:992–9.
27. Burgos JS, Rosol M, Moats RA, et al. Time course of bioluminescent signal in orthotopic and heterotopic brain tumors in nude mice. Biotechniques 2003;34:1184–8.
28. Friedman HS, Schold SC, Jr., Varia M, Bigner DD. Chemotherapy and radiation therapy of human medulloblastoma in athymic nude mice. Cancer Res 1983;43:3088–93.
29. Friedman HS, Bigner SH, McComb RD, et al. A model for human medulloblastoma. Growth, morphology, and chromosomal analysis *in vitro* and in athymic mice. J Neuropathol Exp Neurol 1983;42:485–503.
30. Friedman HS, Schold SC, Jr., Bigner DD. Chemotherapy of subcutaneous and intracranial human medulloblastoma xenografts in athymic nude mice. Cancer Res 1986;46:224–8.
31. Slagel DE, Feola J, Houchens DP, Ovejera AA. Combined modality treatment using radiation and/or chemotherapy in an athymic nude mouse-human medulloblastoma and glioblastoma xenograft model. Cancer Res 1982;42:812–6.
32. Vachon P, Girard C, Theoret Y. Effects of basic fibroblastic growth factor on the growth of human medulloblastoma xenografts. J Neurooncol 2004;67:139–46.
33. Nelson AL, Algon SA, Munasinghe J, et al. Magnetic resonance imaging of patched heterozygous and xenografted mouse brain tumors. J Neurooncol 2003;62:259–67.
34. Schabet M, Martos J, Buchholz R, Pietsch T. Animal model of human medulloblastoma: clinical, magnetic resonance imaging, and histopathological findings after intra-cisternal injection of MHH-MED-1 cells into nude rats. Med Pediatr Oncol 1997;29:92–7.
35. Yang WQ, Senger D, Muzik H, et al. Reovirus prolongs survival and reduces the frequency of spinal and leptomeningeal metastases from medulloblastoma. Cancer Res 2003;63:3162–72.
36. Blaheta RA, Cinatl J, Jr. Anti-tumor mechanisms of valproate: a novel role for an old drug. Med Res Rev 2002;22:492–511.
37. Li XN, Shu Q, Su JM, Perlaky L, Blaney SM, Lau CC. Valproic acid induces growth arrest, apoptosis, and senescence in medulloblastomas by increasing histone hyperacetylation and regulating expression of p21Cip1, CDK4, and CMYC. Mol Cancer Ther 2005;4:1912–22.
38. Waha A, Waha A, Koch A, et al. Epigenetic silencing of the HIC-1 gene in human medulloblastomas. J Neuropathol Exp Neurol 2003;62:1192–201.
39. Pietsch T, Scharmann T, Fonatsch C, et al. Characterization of five new cell lines derived from human primitive neuroectodermal tumors of the central nervous system. Cancer Res 1994;54:3278–87.
40. Li XN, Parikh S, Shu Q, et al. Phenylbutyrate and phenylacetate induce differentiation and inhibit proliferation of human medulloblastoma cells. Clin Cancer Res 2004;10:1150–9.
41. Liu Y, Saad RS, Shen SS, Silverman JF. Diagnostic value of microtubule-associated protein-2 (MAP-2) for neuroendocrine neoplasms. Adv Anat Pathol 2003;10:101–6.
42. Katsetos CD, Legido A, Perentes E, Mork SJ. Class III β-tubulin isotype: a key cytoskeletal protein at the crossroads of developmental neurobiology and tumor neuropathology. J Child Neurol 2003;18:851–66.
43. Lampson LA. New animal models to probe brain tumor biology, therapy, and immunotherapy: advantages and remaining concerns. J Neurooncol 2001;53:275–87.
44. Lindsey JC, Lusher ME, Anderton JA, et al. Identification of tumour-specific epigenetic events in medulloblastoma development by hypermethylation profiling. Carcinogenesis 2004;25:661–8.
45. Lee SH, Kang HS, Rhee CH, et al. Growth-inhibitory effect of adenovirus-mediated p53 gene transfer on medulloblastoma cell line, Daoy, harboring mutant p53. Childs Nerv Syst 2001;17:134–8.
46. Bhowmick NA, Moses HL. Tumor-stroma interactions. Curr Opin Genet Dev 2005;15:97–101.
47. Furukawa T, Fu X, Kubota T, Watanabe M, Kitajima M, Hoffman RM. Nude mouse metastatic models of human stomach cancer constructed using orthotopic implantation of histologically intact tissue. Cancer Res 1993;53:1204–8.
48. Sun FX, Sasson AR, Jiang P, et al. An ultra-metastatic model of human colon cancer in nude mice. Clin Exp Metastasis 1999;17:41–8.
49. Hoffman RM. Orthotopic metastatic (MetaMouse) models for discovery and development of novel chemotherapy. Methods Mol Med 2005;111:297–322.

Clinical Cancer Research

Correction: Valproic Acid Prolongs Survival Time of Severe Combined Immunodeficient Mice Bearing Intracerebellar Orthotopic Medulloblastoma Xenografts

In the Materials and Methods section of this article (Clin Cancer Res 2006;15:4687–94), which was published in the August 1, 2006, issue of *Clinical Cancer Research* (1), the word "coronal" should be "lambdoid." The authors regret this error.

Reference

1. Shu Q, Antalffy B, Su JM, Adesina A, Ou CN, Pietsch T, et al. Valproic acid prolongs survival time of severe combined immunodeficient mice bearing intracerebellar orthotopic medulloblastoma xenografts. Clin Cancer Res 2006;15:4687–94.

Published OnlineFirst March 16, 2012.
doi: 10.1158/1078-0432.CCR-12-0650

Clinical Cancer Research

Valproic Acid Prolongs Survival Time of Severe Combined Immunodeficient Mice Bearing Intracerebellar Orthotopic Medulloblastoma Xenografts

Qin Shu, Barbara Antalffy, Jack Meng Feng Su, et al.

Clin Cancer Res 2006;12:4687-4694.